

Adjustment to heating, potential vorticity and cyclogenesis

By AARNOUT VAN DELDEN*

Institute for Marine and Atmospheric Sciences, Utrecht University, the Netherlands

(Received 30 December 2002; revised 27 June 2003)

SUMMARY

Solutions of an isentropic coordinate model of the atmosphere, permitting acoustic waves and inertial gravity waves, demonstrate that a vertically symmetric heat source in the troposphere usually induces a vertically asymmetric dipole anomaly in the potential vorticity (PV), with an intense, tall and thin positive (cyclonic) anomaly below a less intense, flat and broad negative (anticyclonic) anomaly. The emergence of this asymmetry is associated with the vertical gradient of the PV, which is an important factor in the local PV budget, even when this gradient is zero initially. The degree of vertical asymmetry of the response to heating depends on the ‘thickness’ (in K) of the heated layer relative to the total heat added. The adjusted balanced state shows little sensitivity to the heating intensity (i.e. the time-scale within which the heat is added), in spite of the existence of large-amplitude waves when the heating is applied very abruptly relative to the adiabatic adjustment time-scale. The surrounding (non-heated) region shows little permanent change due to the process of adjustment as far as PV substance and mass is concerned, and only functions as a transmitter of acoustic waves and inertial gravity waves. The balanced state is sensitive to variations in the horizontal scale of the heat source. The response to heating within a PV stratified region (for example, in the region of the tropopause) is quite subtle. For example, it is shown that a heat source in the tropopause region induces a predominantly anticyclonic wind anomaly.

KEYWORDS: Balance Isentropic coordinate model Potential-vorticity substance

1. INTRODUCTION

The adjustment of the atmosphere to internal heating is relevant to the understanding of cyclogenesis due to latent-heat release. Although it is a classical problem in dynamical meteorology, several interesting questions concerning this problem remain to be investigated and answered. These questions can best be stated after introducing the following thought experiment, following Haynes and McIntyre (1987). Imagine that a brief, localized pulse of heating is applied to some region within an unbounded, stably stratified, rotating fluid. Isentropes are depressed locally and, associated with this, mass is transferred across isentropes so that potential vorticity (PV) values are increased below, and decreased above, the location of maximum heating. The subsequent evolution, which is assumed by Haynes and McIntyre to be much slower than the applied heating, involves frictionless, adiabatic adjustment towards thermal wind balance. Inertial gravity waves and acoustic waves are radiated to infinity, and mass and PV substance (PVS) are redistributed along isentropic surfaces until the balanced state is reached, with cyclonic vorticity below and anticyclonic vorticity above the level of maximum heating.

The following questions now arise. To what extent does the heating induce a vertically symmetric dipole in the PV; i.e. a positive (negative) anomaly below (above) the level of maximum heating? Case-studies indicate that the induced PV dipole frequently exhibits a marked vertical asymmetry (Persson 1995; Stoelinga 1996; Wernli and Davies 1997; Pomroy and Thorpe 2000). Does this vertical asymmetry depend on the time-scale of the heating, the heating intensity or other parameters? Can the direct effect of heating or cooling on the PV budget (i.e. the mass flux across isentropes) indeed be viewed independent of the adiabatic adjustment process, even when the heating is applied relatively slowly and gently, i.e. on the same time-scale as the time needed for adjustment? What is the role of waves excited by the heating? Are the fluxes of mass and of PVS from or to the surrounding (non-heated) region during the adjustment process

* Corresponding address: Institute for Marine and Atmospheric Sciences, Utrecht University, Princetonplein 5, 3584 CC Utrecht, the Netherlands. e-mail: a.j.vandelen@phys.uu.nl

small or large? What part of the surrounding region (above, below or beside the heated region) is affected by this exchange of mass and PVS? Will this adiabatic exchange of mass and PVS significantly alter the PV anomaly induced by the heating? How exactly is PVS redistributed *within* the heated region during the adjustment?

The purpose of this paper is to obtain answers to these questions by performing the experiment described above numerically, using a hydrostatic model of the atmosphere with potential temperature as the vertical coordinate. We explicitly address the effect of inertial gravity waves, an effect which was neglected in previous studies (Schubert and Alworth 1987; Möller and Smith 1994; Wirth 1995).

The content of this paper is as follows. After giving some theoretical background in section 2, we continue in section 3 by describing the isentropic coordinate model and the design of the numerical experiments. In section 4 we present a detailed analysis of the budget of mass and of PVS associated with the response to a tropospheric heat source in an atmosphere which is initially at rest. In section 5 we further analyse the reasons for the vertical asymmetry of this response. Section 6 gives an overview of some sensitivity studies. The paper is concluded in section 7 with a summary of the principal results.

2. THEORETICAL BACKGROUND

We make the following simplifying assumptions: the Coriolis parameter, f , is regarded as a constant and the forcing and the response are assumed to be axisymmetric. We, therefore, need only to examine the structure of the flow in the radius-height plane. If we further assume hydrostatic balance, it is convenient to use potential temperature (θ) as vertical coordinate. Hydrostatic balance is then expressed as (Holton, 1992):

$$\frac{\partial \Psi}{\partial \theta} = \Pi, \quad (1)$$

where Ψ is the isentropic stream function, defined according to $\Psi = C_p T + gz$, with C_p the specific heat at constant pressure, T the temperature, g the acceleration due to gravity, z the height of the isentropic surface and Π the Exner function defined according to $\Pi = C_p T / \theta$.

The time-dependent equations of motion and the continuity equation in cylindrical/isentropic coordinates (r, θ) , where r is the radius, are (Anthes 1971):

$$\frac{d(rv)}{dt} = -rfu, \quad (2a)$$

$$\frac{du}{dt} = -\frac{\partial \Psi}{\partial r} + v \left(f + \frac{v}{r} \right), \quad (2b)$$

$$\frac{d\sigma}{dt} = -\sigma \left(\frac{1}{r} \frac{\partial(ru)}{\partial r} + \frac{\partial}{\partial \theta} \frac{d\theta}{dt} \right), \quad (2c)$$

where σ is the inverse of the static stability ($= -g^{-1} \partial p / \partial \theta$), u is the radial velocity, v is the azimuthal velocity (positive if the flow is cyclonic, negative if the flow is anticyclonic) and $d/dt = \partial/\partial t + u\partial/\partial r + (d\theta/dt)\partial/\partial\theta$. The radial derivative is taken at constant θ . The vertical ‘velocity’ in isentropic coordinates is:

$$\frac{d\theta}{dt} = \frac{Q}{\Pi}. \quad (2d)$$

where Q is the heating per unit mass, per unit time.

From (2a) we find that $dM_a/dt = 0$, where $M_a \equiv rv + fr^2/2$ is the angular momentum per unit mass. This implies that M_a is materially conserved, even in the presence of heating.

It is easily deduced from (2a) and (2c) that

$$\frac{dZ_\theta}{dt} = Z_\theta \frac{\partial}{\partial \theta} \left(\frac{d\theta}{dt} \right) - \frac{1}{\sigma} \frac{\partial v}{\partial \theta} \frac{\partial}{\partial r} \left(\frac{d\theta}{dt} \right), \quad (3a)$$

or

$$\frac{\partial Z_\theta}{\partial t} = Z_\theta \frac{\partial}{\partial \theta} \left(\frac{d\theta}{dt} \right) - \frac{1}{\sigma} \frac{\partial v}{\partial \theta} \frac{\partial}{\partial r} \left(\frac{d\theta}{dt} \right) - \frac{d\theta}{dt} \frac{\partial Z_\theta}{\partial \theta} - u \frac{\partial Z_\theta}{\partial r}, \quad (3b)$$

where Z_θ is the PV, defined as

$$Z_\theta \equiv \frac{\zeta_\theta + f}{\sigma}, \quad (4)$$

where $\zeta_\theta = \partial v / \partial r + v/r$ is the relative vorticity. According to (3a), PV is materially conserved if there are no heat sources (remember we have neglected friction).

The local PV budget is made up of the following terms (3b):

$$\begin{aligned} \text{term 1} &= Z_\theta \frac{\partial}{\partial \theta} \frac{d\theta}{dt}; & \text{term 2} &= -\frac{1}{\sigma} \frac{\partial v}{\partial \theta} \frac{\partial}{\partial r} \frac{d\theta}{dt}; \\ \text{term 3} &= -\frac{d\theta}{dt} \frac{\partial Z_\theta}{\partial \theta}; & \text{term 4} &= -u \frac{\partial Z_\theta}{\partial r}. \end{aligned} \quad (5)$$

The sum of terms 1, 2 and 3 is called the *diabatic PV forcing* (Edouard *et al.* 1997). Term 4 represents advection of PV along isentropes and is called *adiabatic PV forcing*. In an atmosphere at rest the only non-zero terms, prior to any adjustment process, are terms 1 and 3. However, term 3 can become non-zero only if the heating is applied in a PV stratified region, where $\partial Z_\theta / \partial \theta \neq 0$.

At $r = 0$ the budget of PV is determined by terms 1 and 3. It was pointed out by Hoskins *et al.* (1985), that these terms can be combined such that:

$$\text{term 1} + \text{term 3} = Z_\theta \frac{\partial}{\partial \theta} \left(\frac{d\theta}{dt} \right) - \frac{d\theta}{dt} \frac{\partial Z_\theta}{\partial \theta} = Z_\theta^2 \frac{\partial}{\partial \theta} \left(\frac{1}{Z_\theta} \frac{d\theta}{dt} \right). \quad (6)$$

Absolute vorticity can be expressed in terms of M_a as:

$$\zeta_\theta + f = \frac{1}{r} \frac{\partial M_a}{\partial r}. \quad (7)$$

The vorticity equation can be written as follows (Haynes and McIntyre 1987):

$$\frac{\partial(\sigma Z_\theta)}{\partial t} = -\nabla \cdot \mathbf{J}, \quad (8)$$

where, assuming axial symmetry,

$$\mathbf{J} \equiv (u, 0) \sigma Z_\theta + \left(\frac{d\theta}{dt} \frac{\partial v}{\partial \theta}, 0 \right). \quad (9)$$

With the divergence theorem we obtain:

$$\frac{d}{dt} \left(\int_V \sigma Z_\theta dV \right) = \int_A -\mathbf{J} \cdot \mathbf{n} dA, \quad (10)$$

where dV is a ‘volume’ element in x - y - θ space, A is the area enclosing the volume V , and \mathbf{n} is the unit vector perpendicular to the area A . The amount of PV per unit ‘volume’ of x - y - θ space is σZ_θ (Haynes and McIntyre 1987, 1990). Therefore, the quantity between brackets on the left-hand side of (10) is equivalent to the total amount of PVS within the ‘volume’ V . The quantity \mathbf{J} is the flux of PVS. Therefore, the quantity on the right-hand side of (10) represents the net flux of PVS across the edge of volume V . Since the component of \mathbf{J} perpendicular to an isentrope is zero (see (9)), (10) implies that there is no flux of PVS across an isentrope, even in the presence of heating. Therefore, the time rate of change of PVS within a given region bounded by two isentropic surfaces is determined by the flux of PVS at the lateral (vertical) boundary of this volume. Note that this flux of PVS has an adiabatic component (the first term on the right-hand side of (9)) and a diabatic component (second term on the right-hand side of (9)). This suggests that the adjustment process, which is necessarily accompanied by a flux of PVS, is not independent of the heating.

The steady-state solution of (2b) is:

$$v \left(f + \frac{v}{r} \right) = \frac{\partial \Psi}{\partial r}. \quad (11)$$

With (1) this yields the equation for thermal wind balance:

$$\frac{c_p}{\theta} \frac{\partial T}{\partial r} = f_{loc} \frac{\partial v}{\partial \theta}, \quad (12)$$

where $f_{loc} = f + (2v/r)$.

Using the definitions of σ and Z_θ and (12), we can derive the following equation (see Hoskins *et al.* 1985):

$$\frac{\partial}{\partial r} \left\{ \frac{1}{r} \frac{\partial(rv)}{\partial r} \right\} + \frac{Z_\theta}{g} \frac{\partial}{\partial \theta} \left(\rho \theta f_{loc} \frac{\partial v}{\partial \theta} \right) = \sigma \frac{\partial Z_\theta}{\partial r}. \quad (13)$$

The solution of this equation yields the flow pattern, $v(r, \theta)$, which is associated with a specific pattern of the isentropic PV in a balanced axisymmetric cyclone. If $f_{loc} Z_\theta > 0$ then (13) is elliptic. Given the distribution of Z_θ , suitable boundary conditions and some additional assumptions, (13) can be solved for the wind $v(r, \theta)$, for instance by relaxation methods (see e.g. Wirth 2001). The solution of (13), if it is elliptic, indicates that $v(r, \theta)$ differs from zero in the region where the radial gradient of Z_θ differs from zero. If $\partial Z_\theta / \partial r$ is negative, $v > 0$ (cyclonic flow), whereas if $\partial Z_\theta / \partial r$ is positive, $v < 0$ (anticyclonic flow). The amplitude of v is a decaying function of θ outside the region of the PV anomaly. If L is the horizontal scale of the PV anomaly, the associated vertical e-folding ‘distance’, $[\Delta\theta]_R$, of the response in v to this anomaly is:

$$[\Delta\theta]_R \equiv L \sqrt{\frac{\rho \theta f Z_\theta}{g}}. \quad (14)$$

$[\Delta\theta]_R$ is referred to as the ‘Rossby-scale height’ (Hoskins *et al.* 1985). It measures the vertical penetration (in isentropic coordinates) of the balanced flow structure above and below the location of the PV anomaly. The Rossby-scale height near the centre of a PV anomaly with a diameter $L \approx 200$ km, is in the order of 6 to 12 K in the troposphere and the lower stratosphere. If we specify a heat source with a horizontal scale of 200 km, this will induce a PV anomaly with a similar horizontal scale. The vertical scale of the adjustment to this anomaly will also be of the order of 6–12 K. In order to model the response to such a heat source a vertical resolution significantly smaller than the Rossby-scale height is required.

3. DESIGN OF THE NUMERICAL EXPERIMENTS

Equations (1), (2a), (2b) and (2c) are approximated by finite differences on a grid of 59 by 80 points, with a vertical grid ‘distance’ of 2.5 K (i.e. a fraction of the Rossby-scale height) and a stretched grid in the radial direction (see the appendix). The computational domain is defined by $290 \leq \theta \leq 435$ K and $0 \leq r < 12\,796$ km. The large radial extent of the domain ensures that waves reflected at the outer boundary do not contaminate the solution near the centre within 36 h. The earth’s surface is assumed to be an isentropic surface, at which $\theta = \theta_s = 285$ K. The pressure at the earth’s surface at $t = 0$ is 1000 hPa.

The static stability is prescribed by the following formulae:

$$\frac{\partial \theta}{\partial p} = A_1 + B_1(\theta - \theta_s) \quad \text{for } \theta \leq \theta_{TT}; \quad (15a)$$

$$\frac{\partial \theta}{\partial p} = A_2 + B_2(\theta - \theta_{TT}) \quad \text{for } \theta_{TT} < \theta \leq \theta_{TS} (\theta_{TS} > \theta_{TT}); \quad (15b)$$

$$\frac{\partial \theta}{\partial p} = A_3 + B_3(\theta - \theta_{TS}) \quad \text{for } \theta > \theta_{TS}; \quad (15c)$$

with

$$A_2 = A_1 + B_1(\theta_{TT} - \theta_s) \quad \text{and} \quad A_3 = A_2 + B_2(\theta_{TS} - \theta_{TT}),$$

where θ_{TT} is the potential temperature at the level separating the tropopause region from the troposphere, and θ_{TS} is the potential temperature at the level separating the tropopause region from the stratosphere. Here we assume that $\theta_{TT} = 325$ K, $\theta_{TS} = 340$ K, $A_1 = -5.5 \times 10^{-4}$ K Pa $^{-1}$, $B_1 = 0$, $B_2 = -4 \times 10^{-4}$ Pa $^{-1}$ and $B_3 = -25 \times 10^{-6}$ Pa $^{-1}$. With this information we are able to determine the pressure at all isentropic levels using (1). Assuming $f = 10^{-4}$ s $^{-1}$, the PV at $t = 0$ (when the atmosphere is at rest) is constant within the troposphere (0.54 PVU \dagger), and increases to 6.43 PVU in the tropopause region. The dynamical tropopause (where $Z_\theta = 2$ PVU) is located approximately at $\theta = 330$ K ($z = 10\,550$ m).

A pulse of heating, lasting for a time τ , is applied to a confined region in an atmosphere at rest. The heat source is specified according to:

$$\frac{d\theta}{dt} = \frac{Q}{\Pi} = Q_0(\theta) \exp \left\{ - \left(\frac{r}{r^*} \right)^2 \right\}, \quad (16)$$

where $Q_0(\theta)$ specifies the vertical distribution of the heating. The heating according to (16) has a maximum value at $r = 0$, and the amplitude of the heating falls off exponentially with increasing r . The associated e-folding distance is $r = r^*$.

The net latent heat released to the air at any height depends on the difference between condensation and evaporation, and between any freezing and melting at that height. Since evaporation and melting associated with a precipitating cloud occur principally below the cloud, and condensation and freezing principally higher up within the clouds, the net heating will possess a maximum value at a specific height above the cloud base, depending on the vertical extent of the clouds (Tao *et al.* 2001). Here we assume that this maximum is located at $\theta = (\theta_0 + \theta_H)/2$, with $\theta_H > \theta_0$. More specifically, $Q_0(\theta)$ is given by:

$$Q_0(\theta) = \frac{A}{2} \left[1 - \cos \left\{ \frac{2\pi(\theta - \theta_0)}{(\theta_H - \theta_0)} \right\} \right] \quad \text{for } \theta_0 \leq \theta \leq \theta_H, \quad (17a)$$

$\dagger 1$ PVU = 10^{-6} K m 2 kg $^{-1}$ s $^{-1}$.

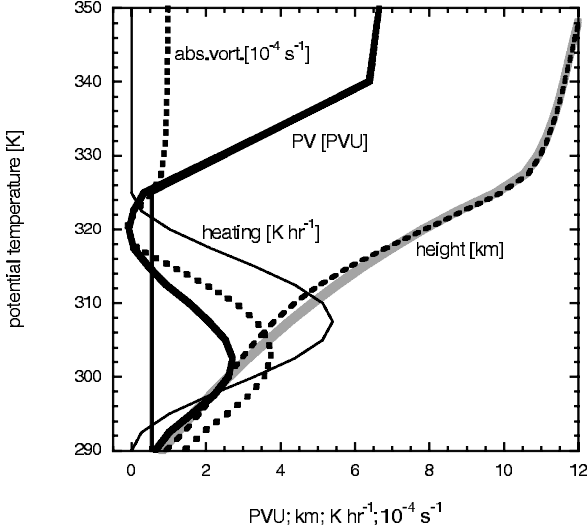


Figure 1. Heating rate between $t = 0$ and $t = 3$ h (very thin solid line), potential vorticity at $t = 0$ (thin solid line) and at $t = 36$ h (thick solid line), height at $t = 0$ (grey line) and at $t = 36$ h (broken line), and absolute vorticity at $t = 3$ h (stippled line) as a function of potential temperature at $r = 0$ ($\tau = 3$ h, $A = 0.0015 \text{ K s}^{-1}$, $\theta_0 = 290 \text{ K}$, $\theta_H = 325 \text{ K}$, $r^* = 100 \text{ km}$ and $f = 10^{-4} \text{ s}^{-1}$). See text for details.

where A is the amplitude (in K s^{-1}) of the heating, and

$$Q_0(\theta) = 0 \quad \text{for } \theta > \theta_H \text{ and for } \theta < \theta_0. \quad (17b)$$

In addition to this, we assume that:

$$Q_0(\theta) = 0 \quad \text{for } r > 2.5 \times r^* \quad \text{and for } t > \tau. \quad (17c)$$

We now investigate the response of the system as a function of the parameters θ_0 , θ_H , r^* , A , τ and f . In all calculations described in sections 4 and 5 we set $r^* = 100 \text{ km}$ and $f = 10^{-4} \text{ s}^{-1}$. The sensitivity of the results to variations in the parameters mentioned above is discussed in section 6.

4. THE BUDGET OF MASS AND PVS DURING ADJUSTMENT TO HEATING

With $\theta_0 = 290 \text{ K}$, $\theta_H = \theta_{TT} = 325 \text{ K}$ and $A = 0.0015 \text{ K s}^{-1}$ (5.4 K h^{-1}), the total heat energy added at $r = 0$ is 4192 W m^{-2} , which is equivalent to a total precipitation of about 6 mm h^{-1} (see the appendix). Figure 1 shows the heating and the height at $r = 0$ as well as the PV at $t = 0$, as a function of potential temperature. Also shown are some results of a numerical experiment with $\tau = 3 \text{ h}$, $A = 0.0015 \text{ K s}^{-1}$ ($A\tau = 16.2 \text{ K}$) and $r^* = 100 \text{ km}$. The variables displayed are PV and height at $t = 36 \text{ h}$ and $r = 0$. Note in particular the vertically asymmetric response of the PV to the vertically symmetric heating. We will discuss this effect in more detail in section 5. Figure 1 also demonstrates that the isentropic surfaces ascend by a few hundred metres (at the most) in the lower troposphere, while they descend in the upper troposphere. Two opposing effects are causing this, namely the heating and the adiabatic temperature decrease associated with upward motion.

The total heat added per unit time to a layer bounded by two isentropes is

$$Q_{\text{tot}} = 2\pi \int_{\theta} \int_r \sigma Q r \, dr \, d\theta. \quad (18)$$

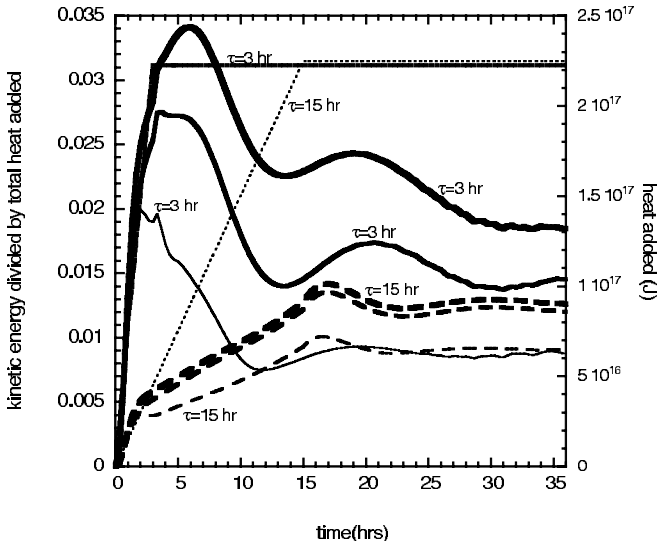


Figure 2. Total heat added and the response of the system, when heating time $\tau = 3$ h and 15 h. In both cases $A\tau = 16.2$ K, $\theta_0 = 290$ K, $\theta_H = 325$ K, $r^* = 100$ km and $f = 10^{-4}$ s $^{-1}$. Response of the system is given in terms of total kinetic energy as a fraction of the total heat added within three regions. The lower curve in each case (indicated by the value of τ) represents the total kinetic energy in a region bounded by $\theta_0 \leq \theta \leq \theta_H$ and $0 \leq r \leq 250$ km (region C in Fig. 3); the middle curve represents the total kinetic energy in a larger region bounded by $\theta_0 \leq \theta \leq \theta_H$ and $0 \leq r \leq 6000$ km; the upper curve represents the total kinetic energy in an even larger region bounded by $\theta_0 \leq \theta \leq 435$ K, and $0 \leq r \leq 6000$ km. See text for further details.

where Q is defined in (16). The total kinetic energy within the same layer is

$$KE_{\text{tot}} = \pi \int_{\theta} \int_r \sigma v^2 r \, dr \, d\theta. \quad (19)$$

In order to diagnose the budget of kinetic energy, mass and PVS we define the following sub-regions: region A is defined by $\theta_0 \leq \theta < (\theta_0 + \theta_H)/2$ and $r < r^*$; region B is defined by $(\theta_0 + \theta_H)/2 \leq \theta \leq \theta_H$ and $r < r^*$; region C is defined by $\theta_0 \leq \theta \leq \theta_H$ and $r < 2.5 \times r^*$; and region D is defined by $\theta_0 \leq \theta \leq \theta_H$ and $r < 5 \times r^*$. Thus, regions A and B represent the inner lower part and the inner upper part of the heated region, respectively, while region C represents the exact total region which is heated.

Figure 2 shows the heat added and also KE_{tot} as functions of time in two experiments, one with $\tau = 3$ h and $A = 0.0015$ K s $^{-1}$, and the other with $\tau = 15$ h and $A = 0.0003$ K s $^{-1}$ (in both cases $A\tau = 16.2$ K and $r^* = 100$ km). Several things should be noted. First: the total kinetic energy generated is a very small fraction (in order of 3%) of the total heat added. Second: the kinetic energy generated within region C after the heating is completed does not depend on the heating intensity, whereas the kinetic energy in the larger domain does depend on the heating intensity. In fact, the additional kinetic energy generated in the case of abrupt heating ($\tau = 3$ hours) is associated with inertial gravity waves, propagating vertically and horizontally away from region C. These waves apparently do not affect the ultimate balanced state reached in the heated region (C).

Figure 3 gives an impression of the movement of isopleths of angular momentum during the first 3 hours of the integration in the numerical experiment with $\tau = 3$ hours and $A\tau = 16.2$ K. Recall that angular momentum is materially conserved, even in the presence of heating (section 2). Initially, the isopleths of angular momentum are

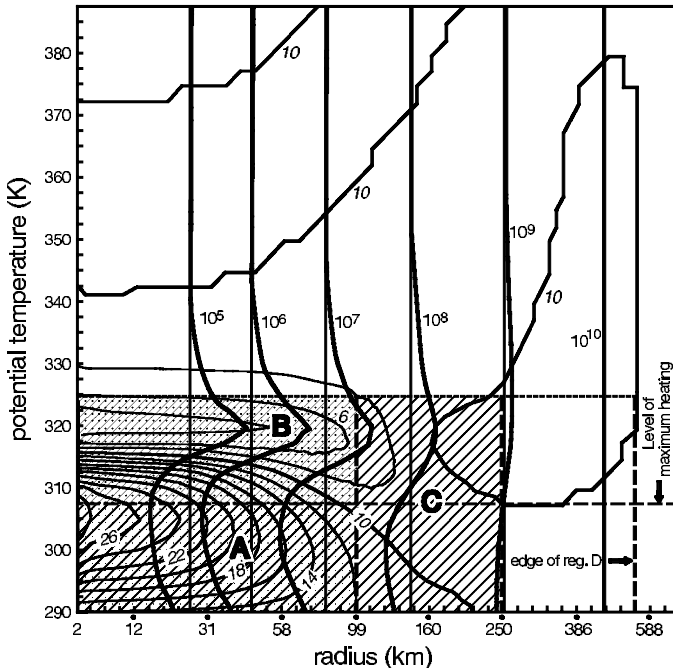


Figure 3. The angular momentum per unit mass (labelled in units of $\text{m}^2 \text{s}^{-1}$) at $t = 0$ (thin solid vertical lines) and at $t = 3 \text{ h}$ (thick solid lines), and absolute vorticity at $t = 3 \text{ h}$ (labelled in units of 10^{-5} s^{-1}). All are given as functions of potential temperature and radius in the case that $\tau = 3 \text{ h}$, $A\tau = 16.2 \text{ K}$, $\theta_0 = 290 \text{ K}$, $\theta_H = 325 \text{ K}$, $f = 10^{-4} \text{ s}^{-1}$ and $r^* = 100 \text{ km}$. Regions A, B and C and the outer edge of region D are indicated (for the precise definition of these regions, see section 4). The radial scale is stretched according to the definition of $r(\mathbf{x})$ given in the appendix. Ticks along the axes correspond to the grid points of the numerical grid. See text for further details.

aligned vertically. The radial displacements of air parcels during the 3-hour period of constant heating are 30 km at the most. An understanding of the mechanism by which a cyclonic circulation arises and intensifies (i.e. the vorticity increases) can be gained by observing the horizontal convergence of isopleths of angular momentum, since the absolute vorticity is proportional to the radial gradient of angular momentum. The convergence of isopleths of angular momentum is greatest just below the level of maximum heating, exactly where the maximum positive anomaly in vorticity is observed at $t = 3 \text{ hours}$. Note that the positive vorticity anomaly has a greater amplitude and vertical extent than the negative vorticity anomaly (Fig. 3).

The changes in the pattern of vorticity are due to adjustment to diabatically induced local changes in PV which, in turn, are due to the dilution or concentration of PVS between isentropic surfaces due to the diabatically induced cross-isentropic flux of mass. The adjustment to balance involves radial motion, which redistributes mass and PVS in order to re-establish balance.

Figure 4 shows the evolution of the total mass, calculated according to

$$M_{\text{tot}} = 2\pi \int_{\theta} \int_r \sigma r \, dr \, d\theta, \quad (20)$$

relative to the initial value within regions A, B, C and D for the case with $\tau = 15 \text{ h}$, $r^* = 100 \text{ km}$ and $A\tau = 16.2 \text{ K}$. The changes are determined by the cross-isentropic mass flux associated with the heating, and by the radial mass flux associated with

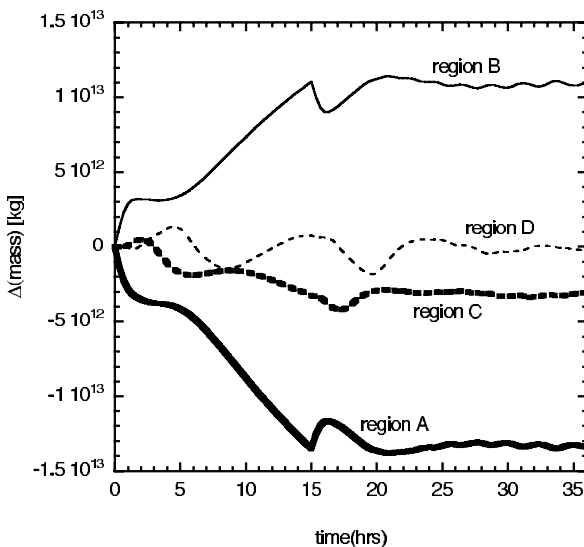


Figure 4. The change in the total mass within regions A, B, C and D (defined in section 4) as a function of time in the integration with $\tau = 15$ h, $A\tau = 16.2$ K, $\theta_0 = 290$ K, $\theta_H = 325$ K, $r^* = 100$ km and $f = 10^{-4}$ s $^{-1}$. See text for definitions.

the adiabatic adjustment. Initially, mass is transported upward across isentropes due to the heating. Therefore the total mass in region A decreases while the total mass in region B increases. This effect is partly compensated by isentropic mass flux divergence. At $t = 15$ h the heating is switched off, the effect of which is seen clearly in Fig. 4. At $t = 0$ the total amount of mass within regions A, B, C and D, is 1.1×10^{14} , 1.1×10^{14} , 1.4×10^{15} and 5.5×10^{15} kg, respectively. After 36 hours, when the system is in an approximate steady state, the heated region (region C) has lost approximately 0.2 % of its mass to the surroundings. In region D there is practically no net loss of mass after 36 hours. The fractional mass changes in regions A and B after 36 hours are much more substantial (about 10%). The exact values, of course, depend on the net heating (2.2×10^{17} J in this case). The important conclusion here is that the net fractional adiabatic mass exchange between the heated region (C) and the environment is very small.

Figure 5 shows the total PVS, calculated according to:

$$PVS_{\text{tot}} = 2\pi \int_{\theta} \int_r \sigma Z_{\theta r} dr d\theta, \quad (21)$$

in regions A, B and C, relative to the initial values. There is a net positive flux of PVS *from* the surrounding reservoir of cyclonic PVS into region A, while there is a net positive flux of PVS *to* the surroundings from region B. After 36 hours the total PVS in region C is practically unchanged compared to the initial value (7.5×10^8 m 2 K s $^{-1}$). Regions A and B each contain the same amount of PVS initially (5.9×10^7 m 2 K s $^{-1}$). The fractional change in the total PVS in these regions is more than 50%. This implies that the redistribution of PVS during adjustment to balance is almost exclusively limited to the heated region (C). Figure 5 also demonstrates that the intensity of the heating (represented by τ) hardly determines the PVS change in region A + B.

The flux of PVS at the edge of region C, calculated from the right-hand side of (10), is very small, while there is a relatively large *net positive* flux of PVS into region

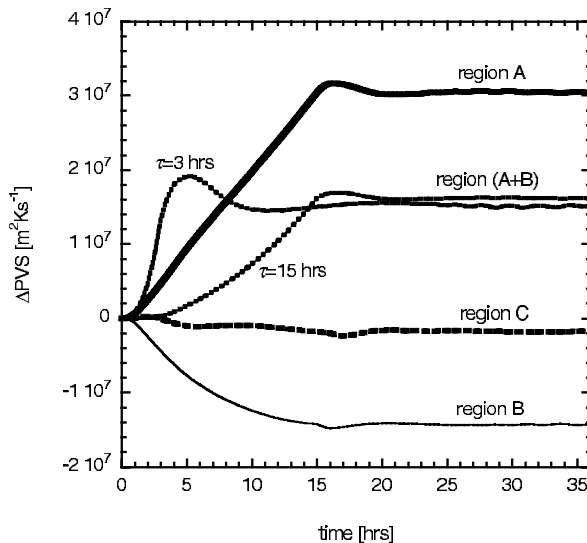


Figure 5. The change in the total potential vorticity substance (PVS) within regions A, B, A + B, and C (defined in section 4) as a function of time. Parameter values are $\tau = 15$ h, $A\tau = 16.2$ K, $\theta_0 = 290$ K, $\theta_H = 325$ K, $r^* = 100$ km and $f = 10^{-4}$ s $^{-1}$. Also shown (second stippled line) is the total PVS in region (A + B) in the case that $\tau = 3$ h and $A\tau = 16.2$ K. See text for definitions.

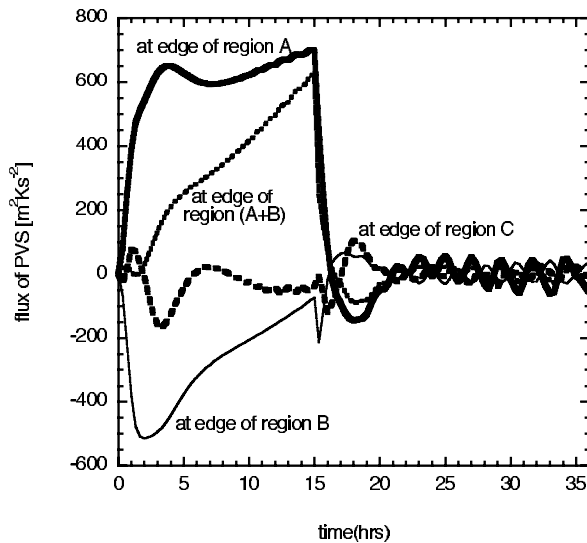


Figure 6. The flux of potential vorticity substance (PVS) at the edge of regions A, B, A + B, and C (defined in section 4) as a function of time. Parameter values are as in Fig. 4.

A + B during the period of heating (Fig. 6). This is associated with the diabatic term in the definition of \mathbf{J} (the second term on the right hand side of (9)), which gives a positive contribution to the tendency in the flux of PVS if $\partial v / \partial \theta < 0$. Assuming thermal-wind balance (12), this corresponds to $\partial T / \partial r < 0$. Therefore, as the central area becomes warmer, and the atmosphere adjusts to balance, this term becomes more effective in contributing to a net positive flux of PVS into the central part of the heated region.

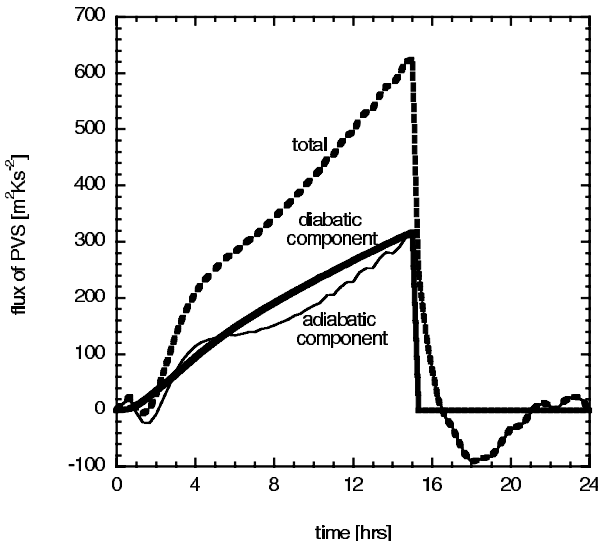


Figure 7. The adiabatic and diabatic components of the flux of potential vorticity substance (PVS) at the edge of region A + B (defined in section 4), and the total flux (also shown in Fig. 6) as a function of time. Parameter values are as in Fig. 4.

In this context it is interesting to note that the diabatic contribution to the flux of PVS is also positive when there is cooling instead of heating, because in that case $\partial T / \partial r > 0$ and, with thermal-wind balance (12), this makes $\partial v / \partial \theta > 0$.

Figure 7 shows the evolution in time of the diabatic and adiabatic contributions to the flux of PVS into region A + B separately. Both these contributions to the flux increase in time during the period of heating. The increase in the adiabatic contribution is due to the increase in PVS values at the edge of region A + B ($r = 100$ km) below the level of maximum heating (where $u < 0$), and the decrease in PVS values at the edge of region A + B above the level of maximum heating (where $u > 0$).

5. VERTICALLY ASYMMETRIC RESPONSE

The response to heating can also be understood by evaluating the local budget of PV, i.e. by evaluating the four terms in (5). At $r = 0$ this budget is determined by terms 1 and 3. However, because $\partial Z_\theta / \partial \theta = 0$ initially in the region where the heating is applied (Fig. 1), only term 1 contributes to the budget of Z_θ at $t = 0$ (Fig. 8(a)). This term gives rise to the well-known symmetric dipole PV anomaly which, assuming thermal-wind balance (12), requires a cyclonic wind anomaly below the level of maximum heating and an anticyclonic wind anomaly above the level of maximum heating. However, the heating alters the vertical stratification of the PV in such a way that $\partial Z_\theta / \partial \theta < 0$ at the level of maximum heating, yielding an additional positive contribution (due to term 3) to the local tendency of Z_θ at this level. Due to this effect, the positive PV anomaly expands upwards (Fig. 8(b)). In the numerical example given here, we find that the net tendency of Z_θ at $r = 0$, just before the heating is turned off (at $t = 3$ h in this case), becomes positive at nearly all heights. Thus, in this sense, heating becomes more effective in intensifying the cyclonic circulation as time progresses.

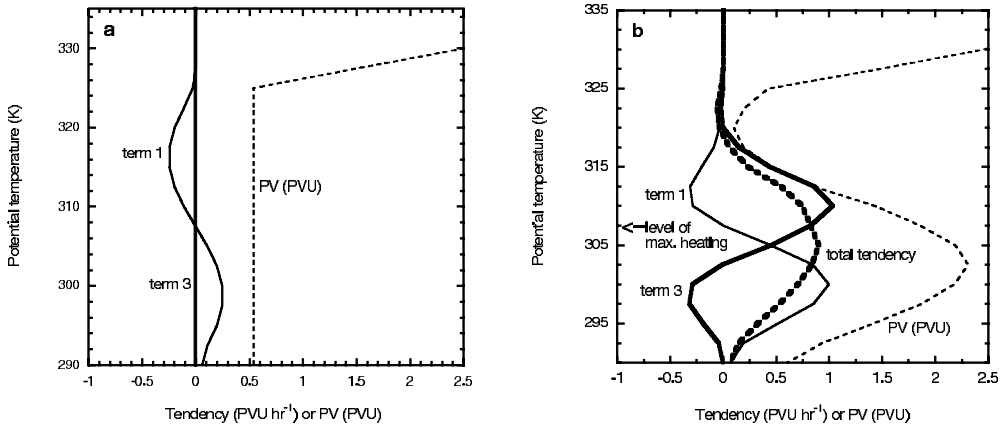


Figure 8. Terms 1 and 3 (see (5)) in the local budget of potential vorticity (PV) at: (a) $r = 0$, $t = 0$ h, and (b) at $r = 0$, $t = 3$ h, as a function of potential temperature. Also shown are the PV and the total tendency of the PV (at $t = 0$ the total tendency is determined by term 1 only). Parameter values are $\tau = 3$ h, $A\tau = 16.2$ K, $\theta_0 = 290$ K, $\theta_H = 325$ K, $r^* = 100$ km and $f = 10^{-4}$ s $^{-1}$. See text for further details.

Wernli and Davies (1997) have hypothesized that the vertical asymmetry of the PV dipole and the associated asymmetric vorticity dipole (Fig. 3) induced by a vertically symmetric heating distribution, depend on the ratio of the time-scale of vertical advection (in the present framework this is $(\theta_H - \theta_0)/(d\theta/dt)$) and the time-scale of the heating (τ). At $r = 0$ this ratio is $2(\theta_H - \theta_0)/A\tau$. The value of this ratio has until now been kept constant at a value of 4.32. Since vertical advection is inducing the vertically asymmetric response to the heating, a small value of this ratio (large τ , i.e. steady heating) would be associated with an asymmetric response, and a large value of this ratio (small τ , i.e. abrupt heating) with a more symmetric response. This hypothesis can therefore be verified by carrying out two additional experiments with constant A and $\Delta\theta$ and different values of τ . The result (Fig. 9) clearly verifies the hypothesis. The degree of asymmetry increases with decreasing value of the ratio $2(\theta_H - \theta_0)/A\tau$.

We must be careful when interpreting this result, because the asymmetry of the response also depends on the background (initial) PV stratification, which is assumed to be zero in the troposphere. In the tropopause region, however, $\partial Z_\theta/\partial\theta$ is large. This has a strong effect on the response to heating, as is demonstrated by the results of a numerical experiment with $A = 0.0003$ K s $^{-1}$, $\tau = 3$ h ($A\tau = 3.24$ K), $r^* = 100$ km, $\theta_0 = 325$ K and $\theta_H = 340$ K. Note that the ratio, $2(\theta_H - \theta_0)/A\tau = 9.26$. In the troposphere this would lead to a strong and tall positive PV anomaly below a weak and flat negative PV anomaly. However, in the tropopause region the response to the vertically symmetric heat source is quite different, i.e. a weak positive anomaly is induced below a strong negative anomaly (Fig. 10).

Figure 10 also demonstrates that the vorticity anomaly, induced by the PV anomaly, is an exponentially decaying function of potential temperature above and below the PV anomaly, in accordance with the solution of (13). The associated e-folding distance in the stratosphere (above the negative anomaly) is about 12 K. This agrees very well with the Rossby-scale height in this region which can be estimated from (14) by substituting a diameter, $L = 2r^* = 200$ km, $g = 10$ m s $^{-2}$, $\rho = 0.3$ kg m $^{-3}$, $\theta = 200$ K, $Z_\theta = 6$ PVU, and $f = 10^{-4}$ s $^{-1}$, which gives $[\Delta\theta]_R \approx 12$ K.

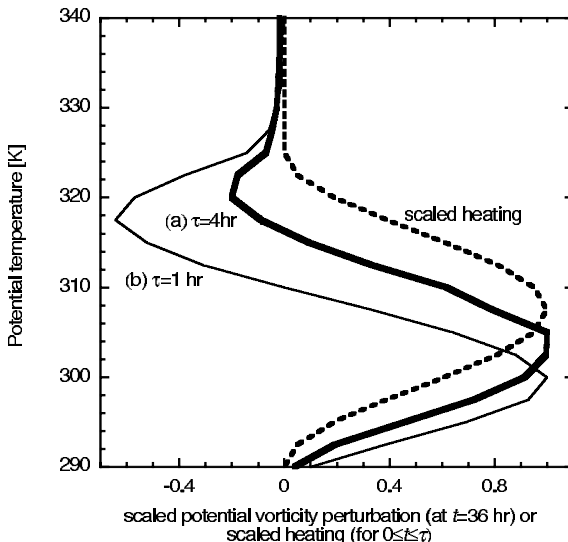


Figure 9. Potential vorticity (PV) perturbation at $r = 0$ and $t = 36$ h (relative to the initial state), scaled with maximum value of the perturbation, in two cases: (a) $2(\theta_H - \theta_0)/A\tau = 3.24$ ($\tau = 4$ h, thick solid line); (b) $2(\theta_H - \theta_0)/A\tau = 12.96$ ($\tau = 1$ h, thin solid line). The maximum value of the PV perturbation is 3.55 PVU in (a), and 0.42 PVU in (b). The heating is also shown (dashed line) scaled with the maximum value (5.4 K h^{-1}). The values of the other parameters were fixed at $A = 0.0015 \text{ K s}^{-1}$, $\theta_0 = 290 \text{ K}$, $\theta_H = 325 \text{ K}$, $r^* = 100 \text{ km}$ and $f = 10^{-4} \text{ s}^{-1}$. See text for further details.

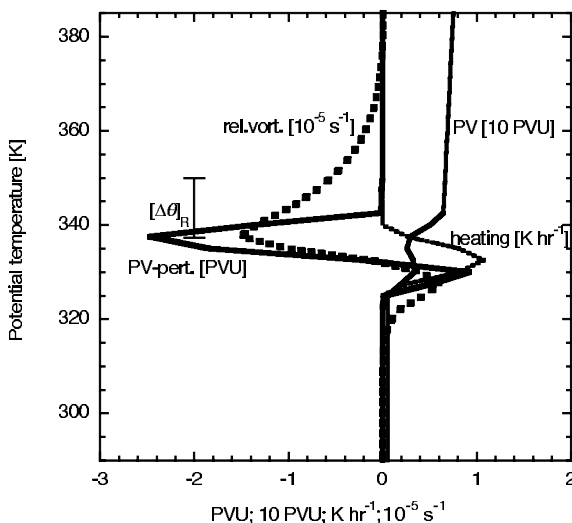


Figure 10. Heating rate (small-dashed line), potential vorticity (PV) at $t = 0$ (thin solid line), PV perturbation at $r = 0$, with $\tau = 3$ h, $A\tau = +3.24 \text{ K}$, $\theta_0 = 325 \text{ K}$, $\theta_H = 340 \text{ K}$, $r^* = 100 \text{ km}$ and $f = 10^{-4} \text{ s}^{-1}$. See text for further details.

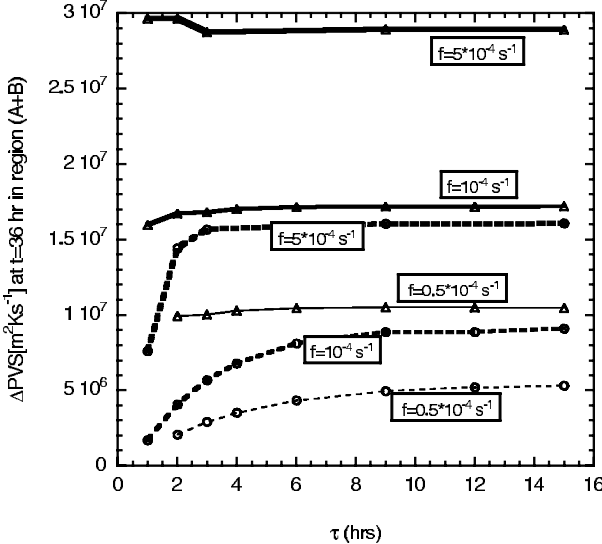


Figure 11. Potential vorticity substance (PVS) within region A + B (defined in section 4) at $t = 36$ h relative to the initial value, as a function of heating time-scale, τ , for three different values of the Coriolis parameter, f (solid lines). The broken lines represent the diabatically induced change of PVS within region A + B at $t = 36$ h relative to the initial value, as a function of τ for the same values of f . Parameter values are $A\tau = 16.2$ K, $\theta_0 = 290$ K, $\theta_H = 325$ K and $r^* = 100$ km. See text for further details.

6. SENSITIVITY TESTS

This section gives an overview of the results of several sensitivity tests and discusses some interesting aspects of these tests. The sensitivity of the response to heating with respect to variations in τ , A (such that $A\tau$ is constant), r^* and f are discussed.

The sensitivity of the response with respect to variations in the intensity of the heating is first investigated by repeating the numerical experiments described in section 4 for different values of τ , each time adjusting the value of A such that $A\tau = 16.2$ K. It appears that the response in terms of the net change in PVS within the inner part of the heated region (region A + B in Fig. 3) after 36 hours of integration is almost identical for all values of τ between 1 and 15 h (Fig. 11). This interesting conclusion clearly does not depend (qualitatively) on the exact value of f . In all cases the PVS exchange with the surrounding non-heated region is negligibly small.

Note that ΔPVS at $t = 36$ h and $f = 10^{-4}$ s $^{-1}$ in Fig. 11 is slightly larger (by about 6%) than the corresponding value plotted in Fig. 5 (for $t = 36$ h). This is due to the fact that ΔPVS in Fig. 11 is computed from the integral:

$$\Delta PVS = 2\pi r^* \int_{t=0}^{t=36 \text{ h}} \int_{\theta_0}^{\theta_H} \left(u\sigma Z_\theta + \frac{d\theta}{dt} \frac{\partial v}{\partial \theta} \right) d\theta dt, \quad (22)$$

(see (9)), whereas ΔPVS in Fig. 5 is computed from (21). This gives an indication of relative numerical error in computing the PVS change within a specific region.

According to (22) the change in PVS is brought about by two effects: an adiabatic effect (ΔPVS_{ad}) associated with the term $u\sigma Z_\theta$, and a diabatic effect (ΔPVS_{diab}) associated with the term $(d\theta/dt) \times (\partial v/\partial \theta)$. The diabatic contribution is plotted in Fig. 11 (the dashed lines) as a function of τ . When τ approaches zero, we find that ΔPVS_{diab} approaches zero (due to the fact that $\partial v/\partial \theta = 0$ at $t = 0$). ΔPVS_{diab} increases

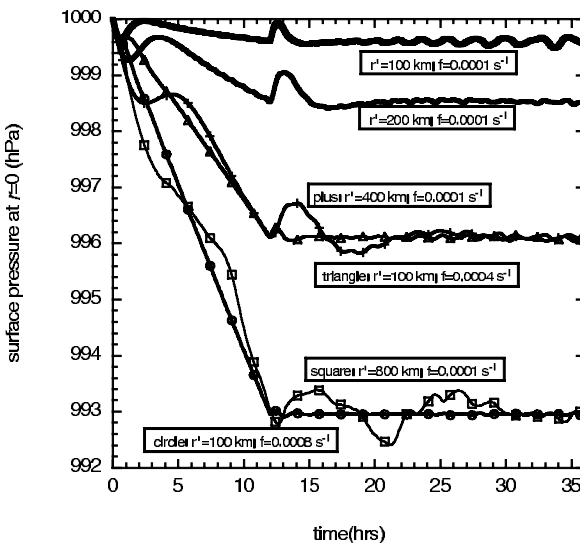


Figure 12. Pressure at the earth's surface ($z = 0$) at $r = 0$ as a function of time for six different combinations of r^* and f . The values of other parameter are $\tau = 12$ h, $A\tau = 16.2$ K, $\theta_0 = 290$ K, $\theta_H = 325$ K. See text for definitions.

with increasing τ and appears to converge asymptotically to a constant value, which depends on the value of f . When τ is small (abrupt forcing) the diabatic contribution to the flux of PVS across the edge of region A + B is relatively small, because the atmosphere is still far from thermal-wind balance during the period of the application of the forcing (when $d\theta/dt \neq 0$), implying that $(\partial v/\partial\theta)$ is relatively small (see (12)). The dashed lines in Fig. 11, thus, contain information about the time-scale of adjustment to thermal-wind balance. Because this time-scale decreases with increasing values of f , ΔPVS_{diab} in Fig. 11 converges much faster to a constant value (with increasing τ) when f is large than when it is small. Stated the other way around: the diabatic contribution to the flux of PVS depends on the time needed for adjustment to thermal-wind balance relative to the forcing time-scale. Since the net change of PVS into region A + B is almost independent of τ , the adiabatic component of the flux of PVS appears to be adjusting to the diabatic component of the flux of PVS.

The sensitivity of the results with respect to variations in the horizontal scale, r^* , of the heat source is tested by repeating the numerical experiment described in section 4 with $\tau = 12$ h and $A\tau = 16.2$ K, for different values of r^* . Figure 12 shows the surface pressure at $r = 0$ as a function of time for different combinations of values for r^* and f . Clearly, the surface pressure at $r = 0$ is sensitive to variations in r^* . This can be understood if we remember that the Rossby-scale height increases with increasing horizontal scale, L , of the PV anomaly (see (14)). Therefore, the anomaly induced by the heating at a certain height above the surface will penetrate further downwards as r^* increases. In view of the expression for the Rossby-scale height (14), an increase in the value of f is expected to have practically the same effect on the surface pressure as an increase in the value of r^* (if $\zeta_0 \ll f$). The numerical solution verifies this expectation (Fig. 12). In general, we may state that the amplitude of the balanced response at the earth's surface increases with increasing ratio of the Rossby-scale height relative to the height of the level of maximum heating above the earth's surface.

7. CONCLUSIONS

This paper presents the results of a numerical investigation into the axisymmetric response of the atmosphere (initially at rest) to internal heating. Although the specified distribution of the heating is rather idealized and not realistic in all respects (it is assumed to be a fixed function of potential temperature, with no heating at the earth's surface and with the level of maximum heating at a fixed isentropic level), this approach certainly yields physical insight into the process of adjustment to heating by specifically yielding answers to the questions posed in the introduction.

We have found that vertically symmetric heating does not usually produce a vertically symmetric dipole anomaly in the (potential) vorticity. The explanation for this is that heating alters the vertical stratification of PV, which is itself an important element in the PV budget. Due to this, a vertically symmetric heat source in the troposphere will induce a relatively deep concentrated cyclone *below* a rather flat broad anticyclone (Fig. 3). Similarly, a vertically symmetric source of cooling in the troposphere will induce a relatively deep concentrated cyclone *above* a rather flat broad anticyclone.

In the tropopause region the response is more complicated and subtle, due to the effect of the background PV gradient. In fact, a heat source in the tropopause region will most likely induce a predominantly negative PV anomaly.

Furthermore, we have found that the net flux divergence of PVS within the heated region during the frictionless adjustment towards thermal-wind balance is practically independent of the intensity of the heating, provided the total heat added is identical in each case. In other words, abrupt heating has practically the same effect on the balanced flow as gentle heating, assuming that the same 'amount' of heat is added in either case. Waves and oscillations have little or no influence on the final balanced state. Therefore the question whether the adiabatic adjustment is much 'slower' than the applied heating, is not of interest for the determination of the balanced state.

The net flux divergence of mass and of PVS to the surrounding non-heated region is negligibly small, even when the amplitude of acoustic and inertial gravity waves, propagating into this region, is significant (i.e. when the heating is applied very abruptly). This implies that the surrounding region is hardly affected permanently by the adjustment.

These conclusions are most interesting for those who seek to incorporate the effect of internal heating, such as latent-heat release, into the 'PV viewpoint' of cyclogenesis, and for those who seek to parametrize heating and cooling in simplified numerical models of the atmosphere (e.g. Montgomery and Enagonio 1998).

The effect of heating at the lower boundary is neglected in this study. A possible next step in this research would involve an attempt to incorporate the effect of heat fluxes at the earth's surface into the PV viewpoint, based on the idea of associating heating at the earth's surface with a flux of PVS.

ACKNOWLEDGEMENTS

I am grateful to Erik Rasmussen who, by inviting me to contribute to a book on polar lows and to give a talk at the EGS in 1999, stimulated me to return to the problem treated in this paper. Discussions with Erik Rasmussen, Theo Opsteegh and Wim Verkley and comments by John Turner have helped clarify my ideas. The very thoughtful criticism given by the reviewers and by the associate editor (Christoph Schär) is also greatly appreciated.

APPENDIX

Details of the method of solution

The solution method of (1) and (2) is similar in many respects to that employed by Anthes (1971). The differences are the higher resolution in the vertical direction and the variable resolution in the radial direction. There are 59 main isentropic levels separated at a constant ‘grid-distance’ of 2.5 K, running from 290 to 435 K. The earth’s surface is also an isentropic level with $\theta = 285$ K. The grid is staggered and stretched in the radial direction. Equation (2c) for σ , is solved on a grid given by:

$$r(x) = b(\exp(\lambda x) - 1),$$

where x is an integer running from 0 to 79, $\lambda = 0.08 \text{ m}^{-1}$ and $b = 25 \times 10^3 \text{ m}$. Equations (2a) and (2b) are solved at intermediate points, i.e. on a grid given by:

$$r_m(x) = b[\exp\{\lambda(x - 0.5)\} - 1].$$

The grid-distance increases from about 2 km between $x = 1$ and $x = 2$ to about 14 km between $x = 25$ and $x = 26$ ($r = 159.8 \text{ km}$), and becomes much larger as x increases further.

The prognostic equations are approximated in space by finite differences, taking into account that $\partial/\partial r = (dx/dr)\partial/\partial x$. Centred differences are used for all the terms except the advection terms, for which the upstream scheme is employed. The resulting equations are integrated in time using the ‘forward–backward’ (or Matsuno) scheme. The boundary conditions are such that the pressure at the highest isentropic level is held constant at the initial value. Furthermore:

$$\begin{aligned} u(r=0) &= 0; & \frac{\partial u}{\partial r}(r \rightarrow \infty) &= 0; & rv(r=0) &= 0; & \frac{\partial rv}{\partial r}(r \rightarrow \infty) &= 0; \\ \frac{\partial \sigma}{\partial r}(r=0) &= 0; & \frac{\partial \sigma}{\partial r}(r \rightarrow \infty) &= 0; & \frac{\partial p}{\partial r}(r=0) &= 0; & \frac{\partial p}{\partial r}(r \rightarrow \infty) &= 0. \end{aligned}$$

The lateral boundary in the model, of course, is at finite distance from the centre. Therefore, the boundary conditions formulated above for the limit of r going to infinity, are applied at this lateral boundary.

The heat added at $r = 0$ is (see (16))

$$Q = Q_0 \Pi \quad (\text{J kg}^{-1} \text{s}^{-1}).$$

This can be converted to a heating rate per square metre ($\text{J s}^{-1} \text{ m}^{-2}$) by multiplying by $\rho \Delta z$, where Δz is the depth of the layer affected by the heating. Using the hydrostatic relation and integrating over the total column yields the total heating rate per square metre, i.e.

$$\text{Total heating} = \sum \sigma_j \Delta \theta_j \bar{\Pi}_j Q_{0j} \quad (\text{W m}^{-2}),$$

where j is the index denoting the layer, $\Delta \theta_j$ is the potential-temperature difference between the top and the bottom of a layer j , $\bar{\Pi}_j$ is the mean value of the Exner function within the layer, and Q_{0j} is the value of Q_0 at level j (see Anthes (1971) for details of the vertical discretization). If we assume that this heating is due to the net effect of condensation of water vapour in clouds and the re-evaporation of rain drops, we can easily translate this into a precipitation, assuming that the latent heat of condensation $L = 2.5 \times 10^6 \text{ J kg}^{-1}$.

REFERENCES

- Anthes, R. A. 1971 A numerical model of the slowly varying tropical cyclone in isentropic coordinates. *Mon. Weather Rev.*, **99**, 617–635
- Edouard, S., Vautard, R. and Brunet, G. 1997 On the maintenance of potential vorticity in isentropic coordinates. *Q. J. R. Meteorol. Soc.*, **123**, 2069–2094
- Haynes, P. H. and McIntyre, M. E. 1987 On the evolution of vorticity and potential vorticity in the presence of diabatic heating and frictional or other forces. *J. Atmos. Sci.*, **44**, 828–841
- Holton, J. R. 1990 On the conservation and impermeability theorems for potential vorticity. *J. Atmos. Sci.*, **47**, 2021–2031
- Hoskins, B. J., McIntyre, M. E. and Robertson, A. W. 1992 *An introduction to dynamic meteorology*. 3rd edition. Academic Press, San Diego, USA
- Möller, J. D. and Smith, R. K. 1985 On the use and significance of isentropic potential vorticity maps. *Q. J. R. Meteorol. Soc.*, **111**, 877–946
- Montgomery, M. T. and Enagonio, J. 1994 The development of potential vorticity in a hurricane-like vortex. *Q. J. R. Meteorol. Soc.*, **120**, 1255–1265
- Persson, P. O. G. 1998 Tropical cyclogenesis via convectively forced Rossby waves in a three-dimensional quasigeostrophic model. *J. Atmos. Sci.*, **55**, 3176–3207
- Pomroy, H. R. and Thorpe, A. J. 1995 Simulations of the potential vorticity structure and budget of Fronts 87 IOP8. *Q. J. R. Meteorol. Soc.*, **121**, 1041–1081
- Schubert, W. H. and Alworth, B. 1987 The evolution and dynamical role of reduced upper-tropospheric potential vorticity in intensive observing period one of FASTEX. *Mon. Weather Rev.*, **128**, 1817–1834
- Stoelinga, M. T. 1996 Evolution of potential vorticity in tropical cyclones. *Q. J. R. Meteorol. Soc.*, **113**, 147–162
- Tao, W.-K., Lang, S., Olson, W. S., Meneghini, R., Yang, S., Simpson, J., Kummerow, C., Smith E. and Halverson, J. 2001 A potential-vorticity-based study of the role of diabatic heating and friction in a numerically simulated baroclinic cyclone. *Mon. Weather Rev.*, **124**, 849–874
- Wernli, H. and Davies, H. C. 1997 Retrieved vertical profiles of latent heat release using TRMM rainfall products for February 1988. *J. Appl. Meteorol.*, **40**, 957–982
- Wirth, V. 1997 A Lagrangian-based analysis of extratropical cyclones. I: The method and some applications. *Q. J. R. Meteorol. Soc.*, **123**, 467–489
- 1995 Diabatic heating in an axisymmetric cut-off cyclone and related stratosphere–troposphere exchange. *Q. J. R. Meteorol. Soc.*, **121**, 127–147
- 2001 Cyclone–anticyclone asymmetry concerning the height of the thermal and the dynamical tropopause. *J. Atmos. Sci.*, **58**, 26–37